X-ray holographic microscopy with zone plates applied to biological samples in the water window using 3rd harmonic radiation from the free-electron laser FLASH

T. Gorniak,[1,*] R. Heine,[1] A. P. Mancuso,[2,8] F. Staier,[1] C. Christophis,[1] M. E. Pettitt,[3] A. Sakdinawat,[4] R. Treusch,[2] N. Guerassimova,[2] J. Feldhaus,[2] C. Gutt,[2] G. Grübel,[2] S. Eisebitt,[5] A. Beyer,[6] A. Gölzhäuser,[6] E. Weckert,[2] M. Grunze,[1,7] I. A. Vartanyants,[2] and A. Rosenhahn[1,7]

[1]*Applied Physical Chemistry, University of Heidelberg, Im Neuenheimer Feld 253, 69120 Heidelberg, Germany*
[2]*HASYLAB at DESY, Notkestr. 85, 22607 Hamburg, Germany*
[3]*School of Biosciences, University of Birmingham, Edgbaston, Birmingham, B15 2TT, United Kingdom*
[4]*Department of Electrical Engineering and Computer Sciences, University of California, Berkeley, CA 94720, USA*
[5]*Institut für Optik und Atomare Physik, Technische Universität Berlin, Straße des 17. Juni 135, 10623 Berlin, Germany*
[6]*Physik supramolekularer Systeme und Oberflächen, Universität Bielefeld, Universitätsstr. 25, 33615 Bielefeld, Germany*
[7]*Institute of Functional Interfaces, Karlsruhe Institute of Technology, Hermann-von-Helmholtz-Platz 1, 76344 Eggenstein-Leopoldshafen, Germany*
[8]*Present address: European XFEL GmbH, Albert-Einstein-Ring 19, 22761 Hamburg, Germany*
**thomas.gorniak@pci.uni-heidelberg.de*

Abstract: The imaging of hydrated biological samples – especially in the energy window of 284-540 eV, where water does not obscure the signal of soft organic matter and biologically relevant elements – is of tremendous interest for life sciences. Free-electron lasers can provide highly intense and coherent pulses, which allow single pulse imaging to overcome resolution limits set by radiation damage. One current challenge is to match both the desired energy and the intensity of the light source. We present the first images of dehydrated biological material acquired with 3rd harmonic radiation from FLASH by digital in-line zone plate holography as one step towards the vision of imaging hydrated biological material with photons in the water window. We also demonstrate the first application of ultrathin molecular sheets as suitable substrates for future free-electron laser experiments with biological samples in the form of a rat fibroblast cell and marine biofouling bacteria *Cobetia marina*.

OCIS codes: (090.1995) Digital holography; (110.7440) X-ray imaging; (030.1640) Coherence; (260.6048) Soft x-rays.

References and links

1. C. A. Brau, "Free-electron lasers," Science **239**(4844), 1115–1121 (1988).
2. J. Feldhaus, J. Arthur, and J. Hastings, "X-ray free-electron lasers," J. Phys. B: At. Mol. Opt. Phys. **38**(9), S799–S819 (2005).
3. W. Ackermann, G. Asova, V. Ayvazyan, A. Azima, N. Baboi, J. Bähr, V. Balandin, B. Beutner, A. Brandt, A. Bolzmann, R. Brinkmann, O. I. Brovko, M. Castellano, P. Castro, L. Catani, E. Chiadroni, S. Choroba, A. Cianchi, J. T. Costello, D. Cubaynes, J. Dardis, W. Decking, H. Delsim-Hashemi, A. Delserieys, G. Di Pirro, M. Dohlus, S. Düsterer, A. Eckhardt, H. T. Edwards, B. Faatz, J. Feldhaus, K. Flöttmann, J. Frisch, L. Fröhlich, T. Garvey, U. Gensch, C. Gerth, M. Görler, N. Golubeva, H. J. Grabosch, M. Grecki, O. Grimm, K. Hacker, U. Hahn, J. H. Han, K. Honkavaara, T. Hott, M. Hüning, Y. Ivanisenko, E. Jaeschke, W. Jalmuzna, T. Jezynski, R. Kammering, V. Katalev, K. Kavanagh, E. T. Kennedy, S. Khodyachykh, K. Klose, V. Kocharyan, M. Körfer, M. Kollewe, W. Koprek, S. Korepanov, D. Kostin, M. Krassilnikov, G. Kube, M. Kuhlmann, C. L. S. Lewis, L. Lilje, T. Limberg, D. Lipka, F. Löhl, H. Luna, M. Luong, M. Martins, M. Meyer, P. Michelato, V. Miltchev, W.

#143770 - $15.00 USD Received 10 Mar 2011; revised 30 Apr 2011; accepted 3 May 2011; published 23 May 2011

D. Möller, L. Monaco, W. F. O. Müller, O. Napieralski, O. Napoly, P. Nicolosi, D. Nölle, T. Nuñez, A. Oppelt, C. Pagani, R. Paparella, N. Pchalek, J. Pedregosa-Gutierrez, B. Petersen, B. Petrosyan, G. Petrosyan, L. Petrosyan, J. Pflüger, E. Plönjes, L. Poletto, K. Pozniak, E. Prat, D. Proch, P. Pucyk, P. Radcliffe, H. Redlin, K. Rehlich, M. Richter, M. Roehrs, J. Roensch, R. Romaniuk, M. Ross, J. Rossbach, V. Rybnikov, M. Sachwitz, E. L. Saldin, W. Sandner, H. Schlarb, B. Schmidt, M. Schmitz, P. Schmüser, J. R. Schneider, E. A. Schneidmiller, S. Schnepp, S. Schreiber, M. Seidel, D. Sertore, A. V. Shabunov, C. Simon, S. Simrock, E. Sombrowski, A. A. Sorokin, P. Spanknebel, R. Spesyvtsev, L. Staykov, B. Steffen, F. Stephan, F. Stulle, H. Thom, K. Tiedtke, M. Tischer, S. Toleikis, R. Treusch, D. Trines, I. Tsakov, E. Vogel, T. Weiland, H. Weise, M. Wellhöfer, M. Wendt, I. Will, A. Winter, K. Wittenburg, W. Wurth, P. Yeates, M. V. Yurkov, I. Zagorodnov, and K. Zapfe, "Operation of a free-electron laser from the extreme ultraviolet to the water window," Nat. Photonics **1**(6), 336–342 (2007).

4. K. Tiedtke, A. Azima, N. von Bargen, L. Bittner, S. Bonfigt, S. Düsterer, B. Faatz, U. Frühling, M. Gensch, C. Gerth, N. Guerassimova, U. Hahn, T. Hans, M. Hesse, K. Honkavaar, U. Jastrow, P. Juranic, S. Kapitzki, B. Keitel, T. Kracht, M. Kuhlmann, W. B. Li, M. Martins, T. Núñez, E. Plönjes, H. Redlin, E. L. Saldin, E. A. Schneidmiller, J. R. Schneider, S. Schreiber, N. Stojanovic, F. Tavella, S. Toleikis, R. Treusch, H. Weigelt, M. Wellhöfer, H. Wabnitz, M. V. Yurkov, and J. Feldhaus, "The soft x-ray free-electron laser FLASH at DESY: beamlines, diagnostics and end-stations," N. J. Phys. **11**(2), 023029 (2009).
5. C. Gutt, L. M. Stadler, S. Streit-Nierobisch, A. P. Mancuso, A. Schropp, B. Pfau, C. M. Günther, R. Könnecke, J. Gulden, B. Reime, J. Feldhaus, E. Weckert, I. A. Vartanyants, O. Hellwig, F. Staier, R. Barth, M. Grunze, A. Rosenhahn, D. Stickler, H. Stillrich, R. Frömter, H. P. Oepen, M. Martins, T. Nisius, T. Wilhein, B. Faatz, N. Guerassimova, K. Honkavaara, V. Kocharyan, R. Treusch, E. Saldin, S. Schreiber, E. Schneidmiller, M. Yurkov, S. Eisebitt, and G. Grübel, "Resonant magnetic scattering with soft x-ray pulses from a free-electron laser operating at 1.59 nm," Phys. Rev. B **79**(21), 212406 (2009).
6. P. Emma, R. Akre, J. Arthur, R. Bionta, C. Bostedt, J. Bozek, A. Brachmann, P. Bucksbaum, R. Coffee, F. J. Decker, Y. Ding, D. Dowell, S. Edstrom, A. Fisher, J. Frisch, S. Gilevich, J. Hastings, G. Hays, P. Hering, Z. Huang, R. Iverson, H. Loos, M. Messerschmidt, A. Miahnahri, S. Moeller, H. D. Nuhn, G. Pile, D. Ratner, J. Rzepiela, D. Schultz, T. Smith, P. Stefan, H. Tompkins, J. Turner, J. Welch, W. White, J. Wu, G. Yocky, and J. Galayda, "First lasing and operation of an ångstrom-wavelength free-electron laser," Nat. Photonics **4**(9), 641–647 (2010).
7. M. Altarelli, R. Brinkmann, M. Chergui, W. Decking, B. Dobson, S. Düsterer, G. Grübel, W. Graeff, H. Graafsma, J. Hajdu, J. Marangos, J. Pflüger, H. Redlin, D. Riley, I. Robinson, J. Rossbach, A. Schwarz, K. Tiedtke, T. Tschentscher, I. Vartanyants, H. Wabnitz, H. Weise, R. Wichmann, K. Witte, A. Wolf, M. Wulff, and M. Yurkov, "The European X-Ray Free-Electron Laser. Technical Design Report" (2006), retrieved *http://xfel.desy.de/tdr/tdr/*.
8. H. N. Chapman, "X-ray imaging beyond the limits," Nat. Mater. **8**(4), 299–301 (2009).
9. N. Patel, "Shorter, brighter, better," Nature **415**(6868), 110–111 (2002).
10. E. L. Saldin, E. A. Schneidmiller, and M. V. Yurkov, *The Physics of Free Electron Lasers* (Springer, 1999).
11. R. Neutze, R. Wouts, D. van der Spoel, E. Weckert, and J. Hajdu, "Potential for biomolecular imaging with femtosecond X-ray pulses," Nature **406**(6797), 752–757 (2000).
12. J. Miao, P. Charalambous, J. Kirz, and D. Sayre, "Extending the methodology of X-ray crystallography to allow imaging of micrometre-sized non-crystalline specimens," Nature **400**(6742), 342–344 (1999).
13. J. Miao, K. O. Hodgson, and D. Sayre, "An approach to three-dimensional structures of biomolecules by using single-molecule diffraction images," Proc. Natl. Acad. Sci. U.S.A. **98**(12), 6641–6645 (2001).
14. I. A. Vartanyants, I. K. Robinson, I. McNulty, C. David, P. Wochner, and T. Tschentscher, "Coherent X-ray scattering and lensless imaging at the European XFEL Facility," J. Synchrotron Radiat. **14**(6), 453–470 (2007).
15. H. N. Chapman, A. Barty, M. J. Bogan, S. Boutet, M. Frank, S. P. Hau-Riege, S. Marchesini, B. W. Woods, S. Bajt, W. H. Benner, R. A. London, E. Plönjes, M. Kuhlmann, R. Treusch, S. Düsterer, T. Tschentscher, J. R. Schneider, E. Spiller, T. Möller, C. Bostedt, M. Hoener, D. A. Shapiro, K. O. Hodgson, D. Van der Spoel, F. Burmeister, M. Bergh, C. Caleman, G. Huldt, M. M. Seibert, F. R. N. C. Maia, R. W. Lee, A. Szöke, N. Timneanu, and J. Hajdu, "Femtosecond diffractive imaging with a soft-X-ray free-electron laser," Nat. Phys. **2**(12), 839–843 (2006).
16. J. Miao, J. Kirz, and D. Sayre, "The oversampling phasing method," Acta Crystallogr. D Biol. Crystallogr. **56**(10), 1312–1315 (2000).
17. V. Elser, "Phase retrieval by iterated projections," J. Opt. Soc. Am. A **20**(1), 40–55 (2003).
18. J. R. Fienup, "Iterative method applied to image reconstruction and to computer-generated holograms," Opt. Eng. **19**, 297–305 (1980).
19. S. Marchesini, "A unified evaluation of iterative projection algorithms for phase retrieval," Rev. Sci. Instrum. **78**(1), 011301–011310 (2007).
20. A. P. Mancuso, T. Gorniak, F. Staier, O. M. Yefanov, R. Barth, C. Christophis, B. Reime, J. Gulden, A. Singer, M. E. Pettit, T. Nisius, T. Wilhein, C. Gutt, G. Grübel, N. Guerassimova, R. Treusch, J. Feldhaus, S. Eisebitt, E. Weckert, M. Grunze, A. Rosenhahn, and I. Vartanyants, "Coherent imaging of biological samples with femtosecond pulses at the free-electron laser FLASH," N. J. Phys. **12**(3), 035003 (2010).
21. I. A. Vartanyants, A. P. Mancuso, A. Singer, O. M. Yefanov, and J. Gulden, "Coherence measurements and coherent diffractive imaging at FLASH," J. Phys. At. Mol. Opt. Phys. **43**(19), 194016 (2010).
22. D. Gabor, "A new microscopic principle," Nature **161**(4098), 777–778 (1948).

#143770 - $15.00 USD Received 10 Mar 2011; revised 30 Apr 2011; accepted 3 May 2011; published 23 May 2011

23. A. Rosenhahn, F. Staier, T. Nisius, D. Schäfer, R. Barth, C. Christophis, L.-M. Stadler, S. Streit-Nierobisch, C. Gutt, A. Mancuso, A. Schropp, J. Gulden, B. Reime, J. Feldhaus, E. Weckert, B. Pfau, C. M. Günther, R. Könnecke, S. Eisebitt, M. Martins, B. Faatz, N. Guerassimova, K. Honkavaara, R. Treusch, E. Saldin, S. Schreiber, E. A. Schneidmiller, M. V. Yurkov, I. Vartanyants, G. Grübel, M. Grunze, and T. Wilhein, "Digital in-line holography with femtosecond VUV radiation provided by the free-electron laser FLASH," Opt. Express **17**(10), 8220–8228 (2009).
24. C. Fuhse, C. Ollinger, and T. Salditt, "Waveguide-based off-axis holography with hard X rays," Phys. Rev. Lett. **97**(25), 254801 (2006).
25. I. McNulty, J. Kirz, C. Jacobsen, E. H. Anderson, M. R. Howells, and D. P. Kern, "High-resolution imaging by Fourier transform X-ray holography," Science **256**(5059), 1009–1012 (1992).
26. G. W. Stroke, "Lensless Fourier-transform method for optical holography," Appl. Phys. Lett. **6**(10), 201–203 (1965).
27. S. Eisebitt, J. Lüning, W. F. Schlotter, M. Lörgen, O. Hellwig, W. Eberhardt, and J. Stöhr, "Lensless imaging of magnetic nanostructures by X-ray spectro-holography," Nature **432**(7019), 885–888 (2004).
28. C. M. Günther, B. Pfau, R. Mitzner, B. Siemer, S. Roling, H. Zacharias, O. Kutz, I. Rudolph, D. Schondelmaier, R. Treusch, and S. Eisebitt, "Sequential femtosecond X-ray imaging," Nat. Photonics **5**(2), 99–102 (2011).
29. G. J. Williams, H. M. Quiney, A. G. Peele, and K. A. Nugent, "Fresnel coherent diffractive imaging: treatment and analysis of data," N. J. Phys. **12**(3), 035020 (2010).
30. R. Treusch and J. Feldhaus, "FLASH: new opportunities for (time-resolved) coherent imaging of nanostructures," N. J. Phys. **12**(3), 035015 (2010).
31. J. Kirz, C. Jacobsen, and M. Howells, "Soft X-ray microscopes and their biological applications," Q. Rev. Biophys. **28**(1), 33–130 (1995).
32. A. Rosenhahn, R. Barth, F. Staier, T. Simpson, S. Mittler, S. Eisebitt, and M. Grunze, "Digital in-line soft x-ray holography with element contrast," J. Opt. Soc. Am. A **25**(2), 416–422 (2008).
33. R. Heine, T. Gorniak, T. Nisius, C. Christophis, M. E. Pettitt, F. Staier, T. Wilhein, S. Rehbein, M. Grunze, and A. Rosenhahn, "Digital in-line X-ray holography with zone plates," Ultramicroscopy (in press, uncorrected proof).
34. M. Martins, M. Wellhöfer, J. Hoeft, W. Wurth, J. Feldhaus, and R. Follath, "Monochromator beamline for FLASH," Rev. Sci. Instrum. **77**(11), 115108 (2006).
35. M. Wellhöfer, M. Martins, W. Wurth, A. Sorokin, and M. Richter, "Performance of the monochromator beamline at FLASH," J. Opt. A, Pure Appl. Opt. **9**(7), 749–756 (2007).
36. F. Staier, "Entwicklung, Bau und Test einer UHV Röntgenstreukammer für die digitale In-Line Holographie," PhD Thesis (University of Heidelberg, 2009).
37. N. Guerassimova, (personal communication, 2009).
38. D. Attwood, *Soft X-Rays and Extreme Ultraviolet Radiation: Principles and Applications* (Cambridge University Press, 2007).
39. J. Garcia-Sucerquia, W. B. Xu, S. K. Jericho, P. Klages, M. H. Jericho, and H. J. Kreuzer, "Digital in-line holographic microscopy," Appl. Opt. **45**(5), 836–850 (2006).
40. J. M. Byrd, T. J. Shea, P. Denes, P. Siddons, D. Attwood, F. Kaertner, L. Moog, Y. Li, A. Sakdinawat, and R. Schlueter, "Enabling instrumentation and technology for 21st century light sources," Nucl. Instrum. Methods Phys. Res. A **623**(3), 910–920 (2010).
41. A. Rosenhahn, R. Barth, X. Cao, M. Schürmann, M. Grunze, and S. Eisebitt, "Vacuum-ultraviolet Gabor holography with synchrotron radiation," Ultramicroscopy **107**(12), 1171–1177 (2007).
42. S. Flewett, H. M. Quiney, C. Q. Tran, and K. A. Nugent, "Extracting coherent modes from partially coherent wavefields," Opt. Lett. **34**(14), 2198–2200 (2009).
43. R. Barth, F. Staier, T. Simpson, S. Mittler, S. Eisebitt, M. Grunze, and A. Rosenhahn, "Soft X-ray holographic microscopy of chromosomes with high aspect ratio pinholes," J. Biotechnol. **149**(4), 238–242 (2010).
44. S. Lindaas, M. Howells, C. Jacobsen, and A. Kalinovsky, "X-ray holographic microscopy by means of photoresist recording and atomic-force microscope readout," J. Opt. Soc. Am. A **13**(9), 1788–1800 (1996).
45. W. Eck, A. Küller, M. Grunze, B. Völkel, and A. Gölzhäuser, "Freestanding nanosheets from crosslinked biphenyl self-assembled monolayers," Adv. Mater. (Deerfield Beach Fla.) **17**(21), 2583–2587 (2005).
46. C. T. Nottbohm, A. Beyer, A. S. Sologubenko, I. Ennen, A. Hütten, H. Rösner, W. Eck, J. Mayer, and A. Gölzhäuser, "Novel carbon nanosheets as support for ultrahigh-resolution structural analysis of nanoparticles," Ultramicroscopy **108**(9), 885–892 (2008).
47. A. Turchanin, M. El-Desawy, and A. Gölzhäuser, "High thermal stability of cross-linked aromatic self-assembled monolayers: nanopatterning via selective thermal desorption," Appl. Phys. Lett. **90**(5), 053102 (2007).
48. A. Küller, W. Eck, V. Stadler, W. Geyer, and A. Gölzhäuser, "Nanostructuring of silicon by electron-beam lithography of self-assembled hydroxybiphenyl monolayers," Appl. Phys. Lett. **82**(21), 3776–3778 (2003).
49. C. T. Nottbohm, A. Turchanin, A. Beyer, and A. Gölzhäuser, "Direct e-beam writing of 1 nm thin carbon nanoribbons," J. Vac. Sci. Technol. B **27**(6), 3059–3062 (2009).
50. A. Turchanin, A. Beyer, C. T. Nottbohm, X. Zhang, R. Stosch, A. Sologubenko, J. Mayer, P. Hinze, T. Weimann, and A. Gölzhäuser, "One nanometer thin carbon nanosheets with tunable conductivity and stiffness," Adv. Mater. (Deerfield Beach Fla.) **21**(12), 1233–1237 (2009).

#143770 - $15.00 USD Received 10 Mar 2011; revised 30 Apr 2011; accepted 3 May 2011; published 23 May 2011

51. A. P. Mancuso, A. Schropp, B. Reime, L.-M. Stadler, A. Singer, J. Gulden, S. Streit-Nierobisch, C. Gutt, G. Grübel, J. Feldhaus, F. Staier, R. Barth, A. Rosenhahn, M. Grunze, T. Nisius, T. Wilhein, D. Stickler, H. Stillrich, R. Frömter, H.-P. Oepen, M. Martins, B. Pfau, C. M. Günther, R. Könnecke, S. Eisebitt, B. Faatz, N. Guerassimova, K. Honkavaara, V. Kocharyan, R. Treusch, E. Saldin, S. Schreiber, E. A. Schneidmiller, M. V. Yurkov, E. Weckert, and I. A. Vartanyants, "Coherent-pulse 2D crystallography using a free-electron laser x-ray source," Phys. Rev. Lett. **102**(3), 035502 (2009).

1. Introduction

The most recent step in the development of highly brilliant and coherent X-ray light sources is the evolution from 3rd generation synchrotrons to free-electron lasers (FELs) [1,2]. The free-electron laser in Hamburg (FLASH) [3,4] operates in the extreme ultraviolet regime (XUV) down to 4.15 nm with lasing demonstrated to occur even in the 5th harmonic [5]. Its successors at shorter wavelengths such as the LCLS in the US [6] and the European XFEL [7] – which are expected to reach much higher (keV) photon energies at strongly increased peak brilliance – offer stunning opportunities to scientists who are working in the fields of physics, chemistry, medicine and biology [8,9]. The above FELs which are based on the self-amplified spontaneous emission (SASE) principle [10] have one key property: they provide ultrashort coherent light pulses, with pulse lengths down to a few femtoseconds. These ultrashort X-ray pulses open the door to high resolution imaging with intense radiation at short wavelengths with a single pulse. The ultrashort pulses allow the evasion of conventional resolution limitations set by radiation damage [11]. The availability of these sources stimulates the development of coherent imaging techniques that are capable of tapping the full potential of these 4th generation light sources. Coherent X-ray diffraction imaging (CXDI) [12] is one prominent and successful approach. The theoretical potential [13,14] as well as the practical feasibility [15] of CXDI as a single-pulse experiment have both been demonstrated. However, CXDI is inseparably linked to the so-called phase problem [16]. Its solution relies on sophisticated iterative algorithms that may not always converge to the correct solution. Even though progress in solving the phase problem has been made in the last years [17–19], it remains challenging. At FLASH, recent CXDI data in the 3rd harmonic at a photon energy of 462 eV was recorded, but the phase retrieval was hampered due to the limited coherence length in this case [20,21]. Contrary to CXDI, holography [22] is a coherent projection microscopy technique. Regardless of the specific approach – in-line, off-axis or Fourier transform holography (FTH) [23–28] – all holographic techniques encrypt phase information during the recording process as the photons scattered from the sample interfere with an undisturbed reference wave. As consequence, phase information is encoded in the fringes of the interference pattern on the detector. This allows a direct reconstruction without the need for iterative phase retrieval. Especially attractive but experimentally more demanding are hybrid approaches, which extend the accessible range of spatial frequencies such as Fresnel coherent diffractive imaging (FCDI) [29]. An overview of current experiments on soft X-ray imaging at FLASH can be found in [30].

In order to take full advantage of the potentially radiation-damage-free imaging of biological samples, one has to optimize sample preparation to minimize any alteration of internal structures. This can be done by studying organic material in its natural hydrated, yet frozen, environment. Wavelengths within 2.3-4.3 nm are especially suitable to probe such hydrated samples. In this so-called water window, which is framed by the K-edges of carbon at 284 eV and oxygen at 540 eV respectively, the biologically relevant elements like potassium, calcium and carbon have a significantly shorter absorption length than water [31]. Due to this relative contrast the elemental distribution [32] and concentration within cells can be revealed. At the time of the experiment, FLASH was not yet capable of delivering radiation at fundamental wavelengths in the water window, and as such we used the 3rd harmonic (λ_3 = 2.68 nm) of the fundamental (λ = 8 nm) to explore this region. In this paper we present the first digital X-ray holograms of biological samples that have been recorded in the water window at a free-electron laser using FLASH's 3rd harmonic at λ_3 = 2.68 nm. Since

#143770 - $15.00 USD Received 10 Mar 2011; revised 30 Apr 2011; accepted 3 May 2011; published 23 May 2011

higher harmonics come at the cost of a considerably reduced photon flux, this experimental setup was based on zone plates rather than following our earlier attempts with pinholes [23]. Creating the required divergent light cone with a zone plate increases the total flux seen by the sample by a factor of 10^2-10^4 compared to an experimental approach based on pinholes [33]. This improved efficiency virtually outweighs the reduced photon flux mentioned above and therefore opens up the water window for X-ray in-line holography at FLASH.

2. Experimental setup

The experiments have been carried out at FLASH's high-resolution plane-grating monochromator beamline PG2 [34,35], where we flange-mounted our dedicated vacuum chamber HORST (holographische Röntgenstreuapparatur) [36]. The FEL operated with a 5 Hz pulse train repetition rate with 30 pulses per train and provided an average of $2\text{x}10^9$ photons per pulse at the 3rd harmonic. This corresponds to the wavelength λ_3 = 2.68 nm, which is well inside the water window. As this wavelength was beyond the designed range of operation of the beamline, its transmittance was only $3.5\text{x}10^{-3}$ (optics, pre-mirror cut and grating efficiency) resulting in $7\text{x}10^6$ photons per pulse in average arriving at our experiment with an energy of E = 462 eV. Compared to the 0th order beam (transmittance of $7.5\text{x}10^{-2}$ and FEL intensity of $2.0\text{x}10^9$ photons/pulse), this higher harmonic provides a lower flux by a factor of $1.3\text{x}10^4$ [37]. The nominal width of the beamline focus is 50 µm full width at half maximum (FWHM) in the horizontal and 1 mm in the vertical direction, meaning that the transmittance of a pinhole with 150 nm in diameter (given the wavelength of 2.68 nm and the distance between focal spot and CCD of 600 nm, one would have to use a 150 nm pinhole in order to achieve a full illumination of the detector) would be about $2\text{x}10^{-7}$. Using a pinhole with a diameter of 100 µm (equal to the size of our zone plate) under the same conditions improves the usable flux to $9\text{x}10^{-2}$ of the photons available for imaging. The efficiency of an unsupported Fresnel zone plate can be estimated to have a value of approximately 9% considering the relevant 1st diffraction order only [38]. Taking into account the geometrical and experimental constraints described above, this evaluation shows that our zone plate is roughly 4 orders of magnitude more efficient than an adequate pinhole, compensating for the lower flux when switching from the fundamental wavelength to the 3rd harmonic.

The experimental setup is depicted schematically in Fig. 1. The zone plate consists of 715 zones arranged within a diameter of D_{zp} = 100 µm. The outermost zone has a width of Δr = 35 nm. This leads to the focal length f = 1.3 mm given a wavelength of 2.68 nm. The direct beam was blocked by a central stop with diameter D_{cs} = 20 µm. In the focus of the zone plate's first diffraction order, an order-sorting aperture (OSA) with a diameter of 2 µm was used to obstruct the higher diffraction orders and the directly transmitted X-ray beam.

#143770 - $15.00 USD Received 10 Mar 2011; revised 30 Apr 2011; accepted 3 May 2011; published 23 May 2011

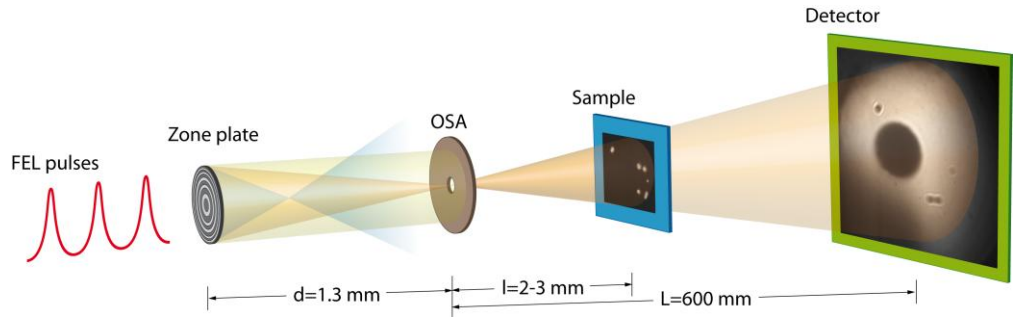

Fig. 1. Schematic drawing of the experimental setup. A zone plate (ZP) is creating the divergent light cone, which is required for digital X-ray holography. An order sorting aperture (OSA) is filtering the direct beam as well as higher diffraction orders from the ZP. To preserve clarity only the 0th (yellow), 1st (orange) and 3rd (blue) diffraction orders are depicted here.

Downstream of the OSA, the samples – the marine bacterium *Cobetia marina* and a rat fibroblast cell – were positioned at distances of 2 and 3 mm, respectively.

The holograms were recorded by a CCD detector (Andor DODX436-BN, 2048x2048 pixels, pixel size: 13.5x13.5 μm^2), which was placed 600 mm behind the zone plate's first diffraction order focus. In this geometry the acquisition time for full saturation of the CCD chip was approximately 600 s. Considering the estimates regarding pinhole transmittances, experiments in the standard pinhole geometry would not have been feasible at the 3rd harmonic. Only the use of zone plate-illumination has enabled these experiments to be carried out.

3. Materials and methods

To reconstruct the holograms we applied the Kirchhoff-Helmholtz transformation, allowing a direct reconstruction of arbitrary image planes between the source of the X-ray cone and the detector without further assumptions about the phase and the sample or iterative refinement [39]:

$$K(\mathbf{r}) = \int_{\text{screen}} I(\boldsymbol{\zeta}) \exp\left[\frac{k\mathbf{r}\boldsymbol{\zeta}}{\zeta}\right] \mathrm{d}x\mathrm{d}y. \qquad (1)$$

The integration extends over the two-dimensional surface of the detector with coordinates $\boldsymbol{\zeta} = (x,y,L)$, where L is the distance from the source (focal spot created by ZP) to the center of the CCD-chip, k is the norm of the wave vector $\mathbf{k}$, and $I(\boldsymbol{\zeta})$ is the measured intensity distribution of the hologram. The wave front $K(\mathbf{r})$ at position $\mathbf{r}$ can be reconstructed at any plane between detector and source in analogy to scanning the focal depth of an optical microscope to display the desired imaging plane within the object. For the numerical implementation of the transformation, a fast algorithm was used that evaluates $K(\mathbf{r})$ analytically. A more detailed overview about reconstruction and resolution in digital in-line holographic microscopy can be found in [39].

All samples were prepared on Si_3N_4-membrane windows purchased from Silson Ltd, Northampton. Rat embryonic fibroblasts REF52WT cells were cultivated on fibrinogen coated silicon nitride membranes (75 nm thick, 1x1 mm^2 window size) for 24 h in Dulbecco's Modified Eagle's Medium (DMEM) supplemented with 10% fetal bovine serum (FBS), both purchased at Gibco. After fixation in 2% paraformaldehyde for 15 min, the cell water was slowly exchanged against ethanol by six different ethanol/water concentrations and the cells were finally critical point dried (Bal-Tec CPD 030). Marine biofouling bacteria *Cobetia marina* were cultivated on membranes with a thickness of 50 nm and a window size of 1x1 mm^2. After immersing the membranes into artificial seawater, *Cobetia marina* bacteria were added and allowed to adhere for 30 min. The adhered organisms were fixed with 2%

#143770 - $15.00 USD Received 10 Mar 2011; revised 30 Apr 2011; accepted 3 May 2011; published 23 May 2011

paraformaldehyde for 15 min and the seawater exchanged against distilled water in six steps. The water was subsequently exchanged against ethanol by six different ethanol/water concentrations and the cells were finally critical point dried (Bal-Tec CPD 030). All samples used in the experiments were characterized by optical microscopy and overview images were recorded. For comparison with the digital in-line X-ray holography images, the corresponding image sections were additionally investigated by reflective and transmission light micrographs (Nikon TE2000, 40x Plan Fluor Ph2, NA = 0.6 and 100x Plan Fluor EPI, NA = 0.9).

The zone plate [40] was prepared using several nanofabrication processes. It was fabricated on a 100 nm thin Si_3N_4-membrane. 5 nm of chromium and 7 nm of gold were evaporated onto the membrane and used as plating base during the gold electroplating process. Polymethyl methacrylate (PMMA) was then spun onto the substrate, and electron-beam lithography was used for generating the zone plate pattern. Then, the PMMA mold was developed and 100 nm thick gold was electroplated to create the zone plate. Afterwards the mold was removed using an oxygen plasma etch. The central beam stop was fabricated with a similar technique in a subsequent step. The theoretical diffraction efficiency of this zone plate in the first order of diffraction is approximately 9% [38]. Taking into account the transmission of the support membrane covered by the chromium and gold layer, approximately 5% of the incoming photons from the beamline were found in the first order focal spot.

4. Results and discussion

Figure 2 shows the first coherent microscopy results of dehydrated biological samples in the water window at a photon energy of E = 462 eV using free-electron laser radiation. Figures 2(a) and 2(b) show scanning electron microscopy images (SEM) of the zone plate, which was used to create the divergent light cone following the schematic drawing of the experiment in Fig. 1. The zone plate's central beam stop is surrounded by periodically arranged virtual Moiré-artifacts due to insufficient sampling of the image. The distance between the zone plate's focal spot and the sample was l = 2 mm. Given the OSA-camera distance of L = 600 mm, this results in a magnification of m = 300.

Figure 2(c) shows an X-ray hologram of the marine bacteria *Cobetia marina* at λ_3 = 2.68 nm. The depicted image is a drift-corrected accumulation of four holograms with an exposure time of 600 s each. As pointed out in the materials and methods section, this is 10^{-4} of the exposure time which would have been required using a pinhole to create a point source with comparable performance. Near the center of the image one can clearly see the dark round shaped spot, which originates from the zone plate's central beam stop. The dashed lines mark the border of regions where the CCD image is dominated by noise. Dividing the pixel-diameters of the inner black spot and the partly visible outer dashed circle we obtain R_{px} = 2750/570 = 4.8. This meets the expectation R = 5 of the ratio of the diameters of the zone plate D_{zp} and the diameter of the central beam stop D_{cs} in real space. Thus the zone plate projects the beam profile out of the ZP-plane onto the CCD. This is why, contrary to our former experimental results, which were based on a setup with pinholes [23], the illumination of the detector does not have the shape of an Airy pattern and also lacks rotational symmetry.

Panel (d) in Fig. 2 shows the reconstructed hologram 2(c) of the biological specimen, a marine bacterium of the genus *Cobetia marina*. A close up of the reconstructed bacterium is shown in Fig. 2(f). The inhomogeneous background in this reconstruction originates from the so-called twin image and the self interference, which contribute to the hologram and are typical for holographic imaging in the soft X-ray range in in-line geometry [41]. For comparison we included a light microscopy image of the same sample region in 2(e). Besides the tight gap between the two bacteria no inner structure can be resolved in the reconstructed hologram. However, a reconstruction is possible, which was not the case with previous CXDI

#143770 - $15.00 USD Received 10 Mar 2011; revised 30 Apr 2011; accepted 3 May 2011; published 23 May 2011

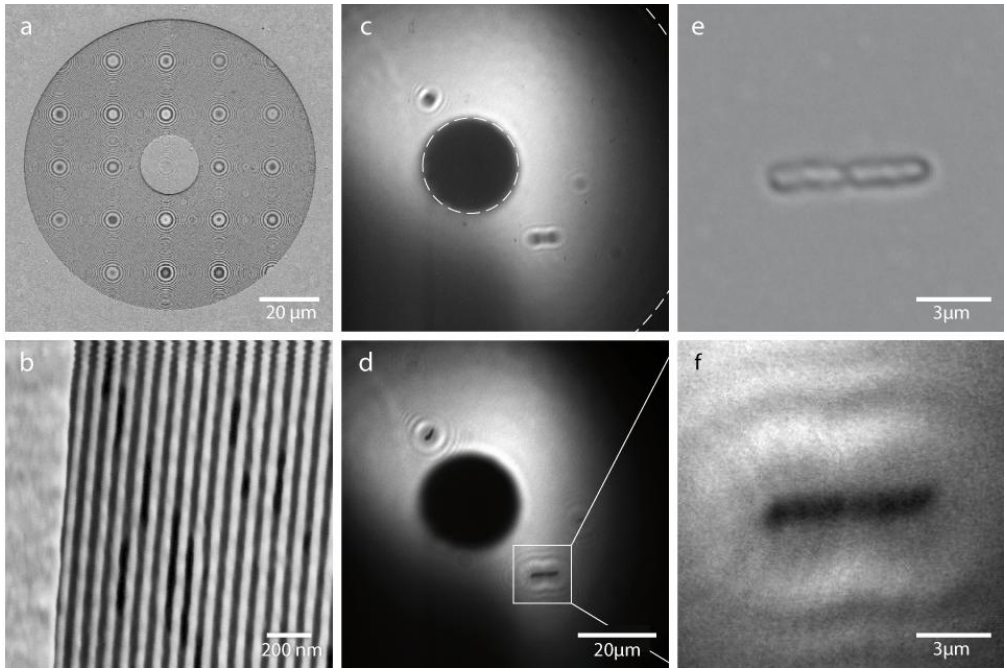

Fig. 2. Imaging the marine bacteria *Cobetia marina* in the water window at λ_3 = 2.68 nm using digital in-line holography. (a) SEM-image of used zone plate with clearly visible central beam stop. (b) Close-up of the zone plate's outermost zones. (c) X-ray hologram with *Cobetia marina* in the lower right corner. (d) Reconstruction of hologram (c). (e) Sample *Cobetia marina* under an optical microscope in bright field illumination (100x, NA = 0.9). (f) Magnified ROI of the reconstructed image as indicated by rectangle in (d).

data in the 3rd harmonic [20]. In the cited CXDI study, insufficient coherence was indicated as the most likely cause for the problems during the reconstruction. Even though there is much effort in the CXDI community to approach the problem of partial coherence [42] – either by knowing the coherence properties of the radiation *a priori*, or by allowing for partial coherence in the iterative reconstruction algorithm – generally, the often used assumption of a fully coherent beam remains problematic to CXDI. In holography, however, limited coherence does not need to be explicitly accounted for and just leads to an image that is lower in quality. Thus, for FEL experiments direct encoding of the phase may be a useful option as a hologram could be used as an initial guess for a hybrid imaging technique like FCDI in order to 'seed' a successful and fast converging high resolution reconstruction even if the data has been acquired under difficult conditions – e.g. a partially coherent source.

Figure 3 shows a critical point dried rat fibroblast cell recorded in the water window at λ_3 = 2.68 nm. Panel (a) contains an overview of the whole cell imaged with an optical microscope in bright field mode. The cell's nucleus with its high contrast is clearly silhouetted against the cytoplasm, which gives only poor contrast and is spread over approximately the whole field of view. Two enlarged regions of interest for resolving further details are shown in the Figs. 3(c) and 3(e). Figure 3(b) depicts the recorded X-ray hologram. Here again – as discussed above – the shadow of the central beam stop and the incomplete illumination can be recognized. To be able to compare our holographic results directly with optical microscopy the hologram 3(b) has been reconstructed and the ROI with the cell nucleus has been magnified in panel (d). Beginning with the nuclear envelope and going further into details inside the nucleus, one can discover a large number of correlations between the images 3(c) and (d). What is more interesting is that the reconstructed X-ray

#143770 - $15.00 USD Received 10 Mar 2011; revised 30 Apr 2011; accepted 3 May 2011; published 23 May 2011

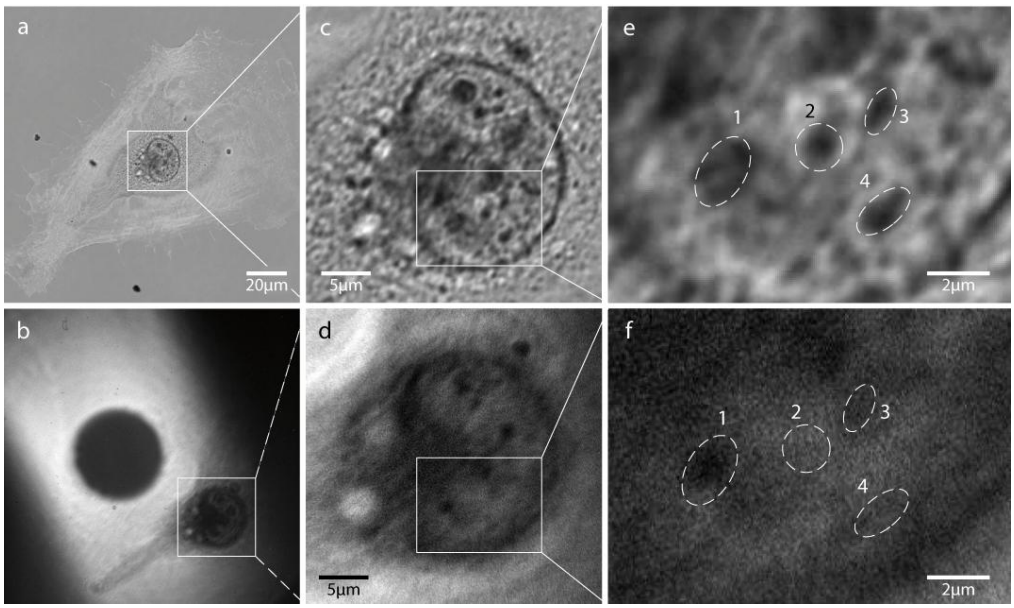

Fig. 3. Imaging a rat's fibroblast cell in the water window at λ_3 = 2.68 nm using digital in-line X-ray holography. (a) Sample imaged with an optical microscope in bright field mode (100x, NA = 0.9). (b) X-ray hologram of the fibroblast (a) at λ_3 = 2.68 nm. The dashed lines indicate that (d) is not a direct magnification of the framed ROI, but its reconstruction. (c) Magnified ROI as indicated in (a) containing the cell nucleus. (d) Reconstructed region with nucleus as indicated in (b). (e) Magnified ROI with nucleoli as marked in (c). (f) Magnified ROI of the X-ray holography image for direct comparison with the optical micrograph in (e).

hologram has some noticeable deviations from the optical micrograph. For a more detailed discussion of this finding we concentrate on four subareas within the ROIs from the images 3(c) and (d), which are magnified in the Figs. 3(e) and 3(f), respectively. The most noticeable difference between the two imaging techniques is the overall contrast level. While the optical microscopy image contains a well-differentiated range of grey values inside the nucleus and thus high contrast, the reconstructed hologram offers a comparable contrast level only on a global scale. The nucleus itself reveals rather weak contrast modulations. Despite this the local contrast behavior promises valuable insights. While the nucleoli – highlighted by dashed oval markers (1-4) – inside the optical micrograph 3(e) all show a comparable grey value, the situation in the reconstructed X-ray hologram 3(f) is markedly different. Here the nucleoli (2) and (4) seem to have disappeared completely and (3) at least partially. Only the nucleolus (1) can be found in both images 3(e) and (f). As discussed in our previous study [32], such a difference can be explained by cellular components with similar optical properties for visible light, but either with a different material density or different chemical composition.

The theoretically achievable resolution is restricted by the experimental setup and the detection geometry. The focus of the zone plate is limited by the outermost zone width of Δr = 35 nm [38]. This determines a theoretical resolution limit of δ_{zp} = 43 nm, as the achievable resolution in point source holography is directly linked to the size of the source of the divergent light cone [43]. The numerical aperture NA_{geo}, which is defined by the sample-detector geometry by the ratio of the size of the CCD over the distance L-l, gives a second, geometrical limit to the achievable spatial resolution. This restriction can be calculated as

$$\delta_{\mathrm{geo}} = 0.61\frac{\lambda_3}{\mathrm{NA}_{\mathrm{geo}}} = 71\mathrm{nm}. \qquad (2)$$

#143770 - $15.00 USD Received 10 Mar 2011; revised 30 Apr 2011; accepted 3 May 2011; published 23 May 2011

In consequence, as the latter exceeds the theoretical limit, the size of the CCD and its distance to the sample sets the relevant resolution limit in the used geometry rather than the focus of the zone plate. The resolution achieved in our experiment was determined by line scans using the 10%/90% edge criterion [41] to be $\delta_{edge} = 485 \pm 88$ nm. This value is the average over the three steepest line plots. They have been measured perpendicular to the edges of an imaged dirt particle, which is situated well above the shadow of the central beam stop. Interestingly, almost every line scan in the vertical direction led to a noticeably poorer resolution. Assuming that this dirt particle does not have perfectly steep knife-edges, the determined value δ_{edge} can be considered as an upper limit of the de facto achieved resolution. Nevertheless, δ_{edge} considerably deviates from the theoretically possible sub-100 nm region. The most likely reason for this is a combined effect of limited coherence, low signal-to-noise ratio (SNR), and poor scattering from the samples. As consequence, coherently small-angle-scattered photons, which are important for high spatial resolution in the reconstruction, were not able to generate a signal strong enough to be interpreted by the reconstruction algorithm. This leads to a reduced effective numerical aperture NA_{eff}. A coarse estimation of NA_{eff} based on the visibility of interference fringes along a line plot across an object leads to a radius of about 160 pixels where one is still able to distinguish the interference signal from the noisy background. This radius translates in our experimental geometry into an effective numerical aperture of $NA_{eff} = 3.3 \times 10^{-3}$, which corresponds to the noise-limited resolution

$$\delta_{\text{eff}} = 0.61\frac{\lambda_3}{\text{NA}_{\text{eff}}} = 453\text{nm}. \qquad (3)$$

Besides the limited data quality due to a low SNR, insufficient temporal coherence can restrict the experimental resolution. A Gaussian fit to the sum of 1857 single shot spectral measurements of the FEL which were recorded just prior to our experiment shows that the distribution of the 3rd harmonic radiation had a maximum at 463 eV with a FWHM of 8 eV. The spatial energy dispersion along the vertical axis in the focal plane was 5.3 eV/mm. Taking into account the zone plate's geometry and the arrangement of the experimental elements, the provided bandwidth corresponds to a coherence length of 2.4 µm and thus should theoretically lead to a temporal coherence-limited resolution of $\delta_{coh} = 584$ nm [44]. While δ_{eff} lies well within the error bar of δ_{edge}, δ_{coh} does not. This difference can be explained by a direction-selective effect, which originates from the orientation of the grating in the monochromator. The calculated value δ_{coh} is only strictly valid in the vertical direction, which resembles the axis of energy dispersion due to the horizontally mounted grating. Thus, temporal coherence should influence the resolution less in the horizontal direction. The aforementioned measurement of the achieved resolution using the edge-criterion already hinted that there may be a direction-selective effect influencing the resolution. Both the line plot for the coarse estimation of the visibility of fringes and the line plots for applying the edge-criterion were not taken in the vertical direction. They rather point to an angle of about 45° against the vertical axis. In consequence, the mismatch of δ_{coh} and δ_{edge} is not astonishing. Since it is rather unlikely that the underlying test object has uniform edges, it is impossible to discriminate between their influence and the impact from the direction-selective coherence. Thus, these results should be considered as a first estimate. According to a study conducted by Vartanyants et al. [21] the influence of the transverse coherence of 3rd harmonic radiation at PG2 does not further decrease the achievable resolution limit set by the temporal counterpart.

While standard silicon nitride membranes supported the imaged biological samples, in recent years novel support materials like carbon nanosheets have been introduced. They provide a substantially thinner yet sufficiently stable support for transmission imaging [45,46]. These support films consist of cross-linked self-assembled monolayers (SAMs) from biphenyl-containing molecules. Their preparation is schematically sketched in Fig. 4(a).

#143770 - $15.00 USD Received 10 Mar 2011; revised 30 Apr 2011; accepted 3 May 2011; published 23 May 2011

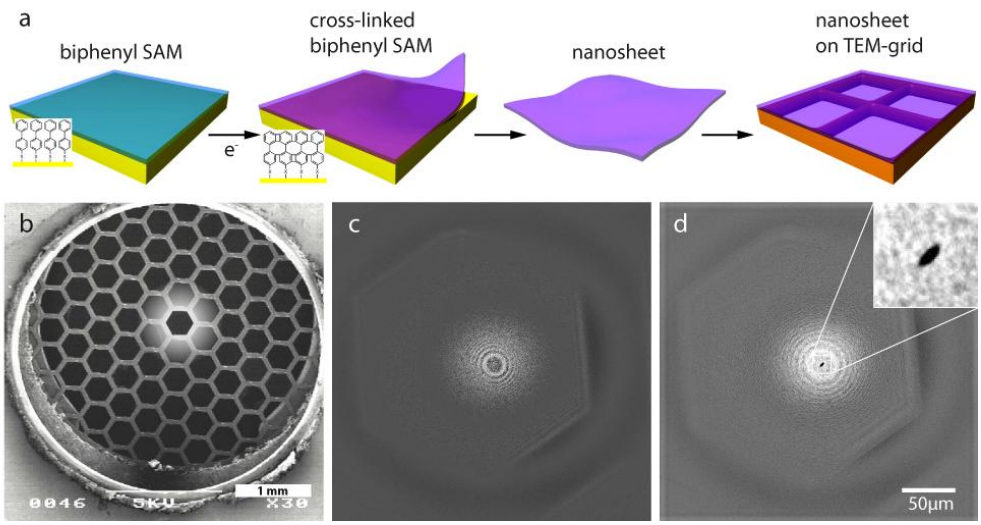

Fig. 4. Carbon nanosheets as a highly transparent substrate for X-ray holography. (a) Schematic fabrication steps consist of cross-linking a biphenyl-based SAM with an electron beam, followed by the transfer of the resulting nanosheet onto a TEM-grid. (b) SEM-image of the TEM-grid over which the nanosheets were spanned. The holographically imaged region is highlighted by a transparent hexagon within a white gradient. (c) X-ray hologram of a dust particle supported by a 1 nm thick carbon nanosheet at E = 155 eV with an exposure time of T = 100 s. The illumination, namely the airy pattern of a 1.2 µm pinhole, has been subtracted. (d) Reconstruction of the hologram with an inset showing the dirt particle in detail. In both, the hologram and its reconstruction, the honeycomb pattern of the TEM-grid is visible.

Electron exposure cross-links the SAM, which leads to an increased stability with respect to high temperatures [47] and acids [48]. In addition an increased mechanical stability allows the release of the monolayer from its substrate, followed by a transfer to a perforated support. In this way openings as large as 225 µm were spanned by a 1 nm thick carbon nanosheet [49,50]. It has been already shown that these support films provide an improved SNR in transmission electron microscopy [46] and is expected that the same will be shown for X-ray microscopy. Here first results are given for X-ray holography. Contrary to earlier results above, the divergent light cone was not generated by a zone plate, but by a pinhole. Furthermore, the photon energy was E = 155 eV, which corresponds to FLASH's fundamental wavelength λ = 8 nm. The SEM-image 4(b) shows the TEM-grid that has been used as a support for the carbon nanosheets. Looking at the grey values one can distinguish covered from uncovered honeycombs. A white hexagon marks the TEM-region, which is fully capped by a nanosheet and has been imaged with X-ray holography. Panel 4(c) shows the recorded hologram of a dirt particle on top of the intact carbon nanosheet. The source has been subtracted in order to make the supporting TEM-grid visible. The acquisition time of the hologram 4(c) was T = 100 s. Its reconstruction is shown in 4(d).

Intensity measurements are consistent with the theoretical prediction of a 99.5% transmittance in the case of a 1 nm thick carbon film at E = 155 eV. Compared to a typical 30 nm Si_3N_4-membrane, this leads to a reduction of the exposure time by a factor of two. These preliminary results show that it is possible to holographically image samples, which are placed on carbon nanosheets. One of the main advantages of such molecular sheets is their small roughness. For imaging of macromolecules or organelles with future X-ray free-electron lasers supported by solid substrates, the roughness of the support will become an increasing challenge for the reconstruction of holographic and CXDI data, as the information lies in the same frequency range as the details to be imaged. Thus, molecular sheets seem to

#143770 - $15.00 USD Received 10 Mar 2011; revised 30 Apr 2011; accepted 3 May 2011; published 23 May 2011

be an ideal support for such experiments including coherent imaging of single proteins, organelles or ordered 2D structures such as membrane systems [51].

5. Conclusions

In summary, we demonstrated, for the first time, the imaging of dehydrated biological material in the water window with radiation from a free-electron laser. The obtained contrast of the dried material is very promising for future experiments on hydrated or vitrified specimen. The implementation of zone plates rather than pinholes allowed us to effectively use 3rd harmonic radiation from FLASH, which provides photons at the desired energy between the K-edges of oxygen and carbon. The insufficient temporal coherence is a challenge on the path to high-resolution holographic imaging in the zone plate geometry – especially given the flux limitations of using the higher harmonics of FELs. To make a successful reconstruction holography may be less demanding on the coherence properties, of the radiation than CXDI is, though at the expense of contrast and resolution. Since higher temporal coherence can be achieved by narrower filtering of the FEL radiation, the attempt of pushing the coherence-limited resolution further up is accompanied by a reduction of photon flux, leading to a drop in the SNR and subsequently in resolution. Thus, the increased photon flux and higher coherence emitted from the currently constructed more powerful light sources like the upgraded FLASH, LCLS or the European XFEL and the option to use photons in the first harmonic are very promising in this respect. A more efficient use of photons by using zone plates in tandem with next generation light sources and new soft X-ray detectors that could offer an enhanced dynamic range and a bigger SNR will be of major importance for high resolution holography. This becomes especially promising if X-ray results obtained on hydrated specimen are considered jointly with other imaging techniques (e.g. correlative microscopy) to solve specific biological questions. Our experiments show that high efficiency zone plates and robust ultrathin substrates can significantly contribute to realizing the vision of single pulse holography of hydrated biological material, where drift related problems and first and foremost limitations set by radiation damage are elegantly overcome with ultrashort flashes. Since FLASH is now capable of delivering photons in the water window at fundamental wavelengths, the vision of imaging hydrated material with high contrast starts to become reality.

Acknowledgments

This work was funded by the BMBF project 05KS7VH1 and 05K10VH4 (FSP 301 FLASH) and by the Office of Naval Research (grant number N00014-08-1-1116). The zone plate work was funded by the U.S. National Science Foundation EUV Engineering Research Center. The authors thank the FLASH machine and experiments team for their great support. We are greatly indebted to the scientific and technical team at FLASH, in particular the machine operators and run coordinators, being the foundation of the successful operation and delivery of the SASE-FEL beam.

#143770 - $15.00 USD Received 10 Mar 2011; revised 30 Apr 2011; accepted 3 May 2011; published 23 May 2011